New Journal of Physics
The open-access journal for physics

Helium–antihydrogen scattering at low energies

S Jonsell[1,4], E A G Armour[2], M Plummer[3], Y Liu[2] and A C Todd[2]

[1] Department of Physics, Stockholm University, SE-10691 Stockholm, Sweden
[2] School of Mathematical Sciences, University of Nottingham, Nottingham NG7 2RD, UK
[3] Computational Science and Engineering, STFC Daresbury Laboratory, Warrington WA4 4AD, UK
E-mail: jonsell@fysik.su.se

New Journal of Physics **14** (2012) 035013 (16pp)
Received 17 November 2011
Published 20 March 2012
Online at http://www.njp.org/
doi:10.1088/1367-2630/14/3/035013

Abstract. We calculate cross sections for helium–antihydrogen scattering for energies up to 0.01 atomic unit. Our calculation includes elastic scattering, direct antiproton–alpha particle annihilation and rearrangement into $He^+\bar{p}$ and ground-state positronium. Elastic scattering is calculated within the Born–Oppenheimer approximation using the potential calculated by Strasburger *et al* (2005 *J. Phys. B: At. Mol. Opt. Phys.* **38** 3091). Matrix elements for rearrangement are calculated using the T-matrix in the distorted wave approximation, with the initial state represented by Hylleraas-type functions. The strong force, leading to direct annihilation, was included as a short-range boundary condition in terms of the strong-force scattering length.

Contents

1. Introduction 2
2. Rearrangement cross sections 2
3. Calculation of the leptonic matrix element 6
4. Elastic and hadronic annihilation cross sections 8
5. Results 11
6. Conclusions 15
Acknowledgment 15
References 15

[4] Author to whom any correspondence should be addressed.

1. Introduction

Research on cold antihydrogen has seen much experimental progress in recent years, including the first demonstration of confinement of antihydrogen in a magnetic trap [1] and the formation of antihydrogen in a cusp trap [2]. Antihydrogen is formed in highly magnetized Rydberg states. Until recently, the antiatoms formed have always been either field ionized, or annihilated against the walls of the experiment, on time scales much shorter than the time needed for relaxing to deeply bound states. This changed very recently when antihydrogen trapping for more than 1000 s was reported by the ALPHA collaboration [3]. Since this time is more than enough for the antiatom to complete the cascade to the ground state, this marks the creation of the first ground-state antiatoms, although the internal states of the trapped antihydrogen could not be measured directly.

The experiments are performed in an environment cooled by liquid helium, but it is not clear at what energies the antihydrogen is formed. Upon formation the antihydrogen has the same kinetic energy as the constituent antiproton had just before the formation event. Although recently antiproton temperatures as low as 9 K were reached by evaporative cooling [4], antihydrogen has so far only been formed at higher temperatures. The antiprotons will, over time, thermalize with the positron plasma with temperatures about 40 K [1]. Since the effective depth of the antihydrogen trap for ground-state atoms is only about 0.5 K only a small fraction of the antihydrogen atoms formed are trapped.

A limit to the lifetime of antihydrogen in the trap is set by collisions with the background gas of ordinary atoms and molecules. This limit comes both from inelastic processes where antihydrogen atoms are destroyed and from elastic scattering where the antihydrogen gains sufficient energy to escape from the trap. Collisions may also change the orbits of the antihydrogen within the trap. Because of the cryogenic system using liquid helium, it is likely that this atom constitutes a significant fraction of the background gas. The temperature of the background gas is unknown, but should fall within the range from liquid helium temperature, 4 K, and room temperature, 300 K. Using the cross sections reported in this paper, it was found in [3] that in this temperature range, and for densities of the background gas estimated from the measured lifetime of antiprotons in the trap, trapping of antihydrogen for times as long as 1000 s is indeed possible.

In order to estimate the possible lifetime of the antihydrogen in the trap, relevant cross sections for He–$\bar{\mathrm{H}}$ scattering are needed within this energy range. While we present cross sections for all relevant processes, the main focus of this paper is the calculation of rearrangement cross sections. The theoretical framework for this calculation is presented in section 2, while the numerical implementation is described in section 3. In section 4, we show how elastic and hadronic annihilation cross sections are calculated from the initial-state interaction potential and the scattering length of the strong nuclear force between the antiproton ($\bar{\mathrm{p}}$) and helium nucleus (α). Our results for all cross sections are presented in section 5 and the conclusions are presented in section 6. We have used atomic units except where other units are explicitly indicated.

2. Rearrangement cross sections

Antihydrogen colliding with helium can undergo a variety of rearrangement processes:

$$\mathrm{He} + \bar{\mathrm{H}} \rightarrow \mathrm{He}^{+}\bar{\mathrm{p}} + \mathrm{Ps}, \tag{1}$$

$$\mathrm{He} + \bar{\mathrm{H}} \rightarrow \mathrm{He}\bar{\mathrm{p}} + e^+, \tag{2}$$

$$\mathrm{He} + \bar{\mathrm{H}} \rightarrow \alpha\bar{\mathrm{p}} + \mathrm{Ps}^-. \tag{3}$$

All rearrangement processes result in the antiproton being bound to the helium nucleus. The ultimate result of these processes will therefore be annihilation, as the complexes formed are metastable. The direct $\bar{\mathrm{H}}$–He annihilation, without the formation of an intermediate metastable complex, requires that the $\bar{\mathrm{p}}$ and α overlap during the collision process. Because of the centrifugal barrier this can only happen for collisions with zero relative angular momentum between the incoming atom and antiatom. Rearrangement, on the other hand, can occur for all relative angular momenta. At collision energies above the ultracold regime, where collisions are not dominated by s-wave scattering ($\gtrapprox 10^{-5}$), rearrangement will therefore be the dominant loss process.

Preliminary results reported earlier [5] showed that the rearrangement into positronium (1) dominates the other rearrangement channels by about two orders of magnitude in the low-energy limit. We shall therefore focus on this process. Our calculation adopts the Born–Oppenheimer approximation for the initial channel, as has previously been done for H–$\bar{\mathrm{H}}$ scattering [6]. In the case of scattering with hydrogen, it has been shown that the Born–Oppenheimer approximation has problems associated with the existence of a critical distance between the colliding nucleus and antiproton, below which the light particles are no longer bound [7, 8]. For the case of scattering with ground-state He, no such critical distance exists, and the Born–Oppenheimer approximation can therefore be expected to work better in this case.

The scattering wavefunction is an eigenfunction of the total Hamiltonian $\hat{H}$,

$$\hat{H}\Psi^{(+)}_{\boldsymbol{k}_\mathrm{i}}(\boldsymbol{R}, \boldsymbol{r}_1, \boldsymbol{r}_2, \boldsymbol{r}_3) = E_\mathrm{i}\Psi^{(+)}_{\boldsymbol{k}_\mathrm{i}}(\boldsymbol{R}, \boldsymbol{r}_1, \boldsymbol{r}_2, \boldsymbol{r}_3). \tag{4}$$

Here, 1 denotes the positron, 2 the electron inside the Ps, 3 the electron left in the $\mathrm{He}^+\bar{\mathrm{p}}$ complex and $\boldsymbol{R} = \boldsymbol{r}_A - \boldsymbol{r}_B$, where A denotes the $\bar{\mathrm{p}}$ and B the He nucleus. The boundary condition used for the scattering wavefunction is an atom and an antiatom colliding with a relative wavevector $\boldsymbol{k}_\mathrm{i}$ and outgoing spherical waves in the final channel. We choose the $\hat{z}$ coordinate along $\boldsymbol{k}_\mathrm{i}$ and make the partial wave expansion

$$\Psi^{(+)}_{\boldsymbol{k}_\mathrm{i}}(\boldsymbol{R}, \boldsymbol{r}_1, \boldsymbol{r}_2, \boldsymbol{r}_3) = \sum_J \Psi^{(+)}_{\varepsilon_\mathrm{i}, J}(R, \boldsymbol{r}_1, \boldsymbol{r}_2, \boldsymbol{r}_3) P_J(\cos\theta_R), \tag{5}$$

where J is the total angular momentum, P_J the Legendre polynomial, ε_i the collision energy, $\varepsilon_\mathrm{i} = k_\mathrm{i}^2/(2\mu) = E_\mathrm{i} - E_{\bar{\mathrm{H}}} - E_\mathrm{He} = E_\mathrm{i} + 3.404$, and μ the reduced mass in the initial channel.

Our calculation uses the T-matrix in the prior form [9]. In this approach, the Hamiltonian of the helium–antihydrogen system is separated as

$$\hat{H} = \hat{H}_0 + V, \tag{6}$$

$$\hat{H}_0 = \hat{H}_{\mathrm{He}^+\bar{\mathrm{p}}} + \hat{H}_\mathrm{Ps} + \hat{T}, \tag{7}$$

$$V = -\frac{1}{r_{A1}} + \frac{2}{r_{B1}} + \frac{1}{r_{A2}} - \frac{2}{r_{B2}} - \frac{1}{r_{13}} + \frac{1}{r_{23}}. \tag{8}$$

$\hat{H}_{\mathrm{He}^+\bar{\mathrm{p}}}$ and $\hat{H}_\mathrm{Ps}$ denote the internal Hamiltonians of the fragments in the final channel, and $\hat{T}$ their relative kinetic energy. V is the interaction between the final-state fragments. The asymptotic wavefunction in the final channel is given by

$$\hat{H}_0\Phi(\boldsymbol{R}, \boldsymbol{r}_1, \boldsymbol{r}_2, \boldsymbol{r}_3) = E_\mathrm{f}\Phi(\boldsymbol{R}, \boldsymbol{r}_1, \boldsymbol{r}_2, \boldsymbol{r}_3). \tag{9}$$

The T-matrix can then be expressed as

$$T_{\rm fi} = \langle \Phi | V | \Psi_{\boldsymbol{k}_{\rm i}}^{(+)} \rangle, \tag{10}$$

and the rearrangement cross section $\sigma_{\rm r}$ is

$$\sigma_{\rm r} = \frac{(2\pi)^4}{\hbar v_i} \int \delta(E_{\rm i} - E_{\rm f}) |T_{\rm fi}|^2 {\rm d}\boldsymbol{k}_{\rm f}, \tag{11}$$

where $v_{\rm i}$ is the relative speed in the initial channel and $\boldsymbol{k}_{\rm f}$ is the relative wavevector between the fragments in the final channel.

For the scattering wavefunction we use the Born–Oppenheimer approximation

$$\Psi_{\varepsilon_{\rm i},J}^{(+)}(R, \boldsymbol{r}_1, \boldsymbol{r}_2, \boldsymbol{r}_3) = \chi_{\varepsilon_{\rm i},J}(R) \psi_{\rm BO}(R; \boldsymbol{r}_1, \boldsymbol{r}_2, \boldsymbol{r}_3), \tag{12}$$

where the Born–Oppenheimer wavefunction is the wavefunction of the light particles with the heavy particles at a fixed R. This is a bound state of all the light particles. The continuum nature of the initial state is captured by the much simpler wavefunction $\chi_{\varepsilon_{\rm i},J}(R)$, which represents the motion of the nuclei. The separation of the most complex part of the calculation, the state of the light particles, into a bound-state problem makes the combination of the prior-form T-matrix and the Born–Oppenheimer approximation particularly useful. Hence, the approximation (12) of $\Psi_{\varepsilon_{\rm i},J}^{(+)}$ does not contain the asymptotic final state. The T-matrix calculated in this approach therefore amounts to the distorted-wave Born approximation.

The final-state wavefunction has the form

$$\Phi(\boldsymbol{R}, \boldsymbol{r}_1, \boldsymbol{r}_2, \boldsymbol{r}_3) = \sqrt{2} \Upsilon_{{\rm He}^+\bar{\rm p}}(\boldsymbol{R}, \boldsymbol{r}_3) \psi_{\rm Ps}(\boldsymbol{\rho}, \boldsymbol{r}_{12}), \tag{13}$$

where $\Upsilon_{{\rm He}^+\bar{\rm p}}(\boldsymbol{R}, \boldsymbol{r}_3)$ is the wavefunction for the ${\rm He}^+\bar{\rm p}$ complex, also calculated in the Born–Oppenheimer approximation, $\Upsilon_{{\rm He}^+\bar{\rm p}}(\boldsymbol{R}, \boldsymbol{r}_3) = \xi(\boldsymbol{R}) \phi_{{\rm He}^+\bar{\rm p}}(\boldsymbol{R}; \boldsymbol{r}_3)$. The function $\psi_{\rm Ps}$ represents the positronium as a function of $\boldsymbol{r}_{12}$, the relative electron–positron coordinate and the center-of-mass motion of the positron, as a function of $\boldsymbol{\rho}$, which is the vector between the mass centers of the two fragments. The factor $\sqrt{2}$ allows for exchange between the electrons [10]. For the final ${\rm He}^+\bar{\rm p}$ state the Born–Oppenheimer potential and its adiabatic correction can be obtained to essentially arbitrary accuracy, since the problem is separable in prolate spheroidal coordinates. Since the final states are bound the long-range part of the potential is not needed. The bound-state energies were obtained by the simple shooting method.

Above, the initial-state wavefunction has been expressed in the body-fixed frame, which rotates with the colliding atom and antiatom. In the final state, on the other hand, it is most convenient to express $\psi_{\rm Ps}$ in the space-fixed frame, which does not rotate. Care has to be taken to transform between these frames when the T-matrix element (10) is calculated. These considerations are considerably simplified by two restrictions of our calculation. First of all, we shall only consider rearrangement into ground-state (1S) positronium. Secondly, we shall approximate the final-state plane wave motion of the positronium by its spherically symmetric part, i.e.

$$\exp({\rm i}\boldsymbol{k}_{\rm f} \cdot \boldsymbol{\rho}) = \sum_{l=0}^{\infty} (2l+1) {\rm i}^l j_l(k_{\rm f}\rho) P_l(\cos\theta_\rho) \simeq \frac{\sin(k_{\rm f}\rho)}{k_{\rm f}\rho}, \tag{14}$$

where j_l are the spherical Bessel functions, P_l the Legendre polynomials and θ_ρ the polar angle of the vector $\boldsymbol{\rho}$. In the united atom limit $R \to 0$ the He–$\bar{\rm H}$ system becomes equivalent to positronium hydride, PsH (a Ps bound to a hydrogen atom). This state is spherically symmetric [11], and hence all terms with $l > 0$ in (14) will in this limit give zero contribution to the T-matrix element. For $R > 0$ the deviation from spherical symmetry of the initial state

Table 1. Binding energies E_b of the final $He^+\bar{p}$ states considered, calculated in the Born–Oppenheimer approximation. The energy $\epsilon_f = E_b - E_{Ps} + (E_{He} + E_{\bar{H}}) = E_b - 3.153725$ is the energy of the center-of-mass motion in the final state for zero collision energy, and k_f the corresponding wavevector. J and v are the rotational and vibrational quantum numbers.

J	v	E_b	ϵ_f	k_f
0	35	3.164 29	0.010 57	0.205 61
1	35	3.164 06	0.010 33	0.203 30
2	35	3.163 58	0.009 86	0.198 58
3	35	3.162 87	0.009 15	0.191 29
4	35	3.161 92	0.008 20	0.181 08
5	35	3.160 73	0.007 01	0.167 42
6	35	3.159 30	0.005 58	0.149 33
7	35	3.157 62	0.003 90	0.124 87
8	35	3.155 70	0.001 97	0.088 88
9	35	3.153 53	−0.000 20	–
10	35	3.151 10	−0.002 62	–
11	35	3.148 41	−0.005 31	–
0	34	3.265 32	0.111 59	0.668 11
0	33	3.378 56	0.224 84	0.948 34

is measured by the quadrupole moment of the leptonic mass distribution, which has been calculated in [12]. Here partial waves up to $l \sim k_f a$ are significant, where a is the effective outer limit of the ρ integration in the evaluation of the T-matrix element. This limit is set by the spatial extent of the wavefunction of the leptons in the initial channel. In our calculations we only consider final $He^+\bar{p}$ states lying close to the scattering threshold. The latter restriction implies that $k_f < 1$ (see table 1). The lepton distribution of the initial state is most diffuse (and hence a is largest) in the $R \to 0$ limit (where the state is spherically symmetric). For PsH the root mean square (rms) value of the electron–proton distance is 2.80 [13], which can be used as an estimate for the maximum of a. For the energy released in the formation of the $v = 35$, $J = 0$ state of $He^+\bar{p}$, this estimate gives $k_f a \sim 0.58$. As R increases a will decrease, and around $R = 1$ the rms value of the $e^- - \alpha$ distance is close to its atomic value 1.54 [12].

With these simplifications the final state becomes

$$\psi_{Ps}(\boldsymbol{\rho}, \boldsymbol{r}_{12}) = \phi_{Ps}^{1s}(r_{12}) \frac{\sin k_f \rho}{k_f \rho}. \tag{15}$$

This expression is spherically symmetric, and hence looks the same in the space fixed and the body-fixed frames. This simplifies our calculation considerably, as a number of angular variables drop out, and the rotational quantum numbers J, M of the initial channel translate into the same quantum numbers for the bound $He^+\bar{p}$ complex, i.e. no angular momentum is carried away by the positronium.

The T-matrix element T_{fi} (10) for the Jth partial wave can now be separated into a leptonic and a nuclear part,

$$T_{fi} = \int \xi^*(\boldsymbol{R}) t_{fi}(R) \chi_{\varepsilon_i, J}(R) P_J(\cos\theta_R) \mathrm{d}\boldsymbol{R}, \tag{16}$$

where $\xi(\boldsymbol{R})$ represents the nuclear motion of the $He^+\bar{p}$ with the same rotational quantum number J as in the initial state, and the leptonic T-matrix is

$$t_{fi}(R) = \langle \psi_{Ps}\phi_{He^+\bar{p}} | V | \psi_{BO} \rangle. \tag{17}$$

3. Calculation of the leptonic matrix element

The main challenge is the calculation of the leptonic matrix elements $t_{fi}(R)$. For a fixed internuclear separation R, the initial leptonic state of the $He\bar{H}$ complex is bound, and hence the Born–Oppenheimer wavefunction $\psi_{BO}(R; \boldsymbol{r}_1, \boldsymbol{r}_2, \boldsymbol{r}_3)$ can be calculated using the Rayleigh–Ritz variational principle.

Our calculation used prolate spheroidal coordinates $(\lambda_i, \mu_i, \phi_i)$ for the light particles, which are defined as

$$\lambda_i = \frac{r_{iA} + r_{iB}}{R}, \tag{18}$$

$$\mu_i = \frac{r_{iA} - r_{iB}}{R}, \tag{19}$$

and ϕ_i is the usual azimuthal angle of spherical polar coordinates. The Cartesian coordinates can be expressed in terms of prolate spheroidal coordinates as

$$x_i = \frac{R}{2}\sqrt{(\lambda_i^2 - 1)(1 - \mu_i^2)}\cos\phi_i, \tag{20}$$

$$y_i = \frac{R}{2}\sqrt{(\lambda_i^2 - 1)(1 - \mu_i^2)}\sin\phi_i, \tag{21}$$

$$z_i = \frac{R}{2}\lambda_i\mu_i. \tag{22}$$

In terms of these coordinates our basis functions take the form

$$\psi_i = (1 + P_{23})\lambda_1^{m_i}\lambda_2^{n_i}\lambda_3^{p_i}\mu_1^{j_i}\mu_2^{k_i}\mu_3^{l_i}C(s_i, t_i)\exp[-\alpha_1\lambda, -\alpha_2\lambda_2 - \alpha_3\lambda_3 + \beta_1\mu_1 + \beta_2\mu_2 + \beta_3\mu_3]. \tag{23}$$

Here P_{23} is the electron permutation operator. For collisions involving He in its ground state the electrons are in a singlet spin state, and thus the overall wavefunction has the required antisymmetric form under electron exchange. The factor $C(s_i, t_i)$ denotes the various types of basis functions according to table 2.

The electron–positron Hylleraas-type functions combined with the electron–electron repulsion r_{23}^{-1} in V give rise to matrix elements of the type $r_{12}r_{13}/r_{23} = r_{12}^2 r_{13}^2/(r_{12}r_{13}r_{23})$. Factors of the type r_{ij}^2 can easily be expressed in prolate spheroidal coordinates, while $1/r_{ij}$ factors are handled using the Neumann expansion

$$\frac{1}{r_{ij}} = \frac{2}{R}\sum_{\tau=0}^{\infty}\sum_{\nu=0}^{\tau} P_\tau^\nu(\lambda_<)Q_\tau^\nu(\lambda_>)P_\tau^\nu(\mu_i)P_\tau^\nu(\mu_j)\cos[\nu(\phi_i - \phi_j)]. \tag{24}$$

Here $\lambda_<$ is the lesser, and $\lambda_>$ the greater, of λ_i and λ_j. $P_\tau^\nu(\lambda)$ and $Q_\tau^\nu(\lambda)$ are solutions to the Legendre equation (associated if $\nu \neq 0$).

Hence, a triple Neumann expansion was required. It was found that integration over all the ϕ and μ coordinates, as well as one of the λ coordinates, could be carried out analytically.

Table 2. Types of basis functions used in the He–$\bar{\text{H}}$ calculations.

s_i	t_i	$C(s_i, t_i)$	Type
0	0	1	Product of σ functions
1	1	r_{12}	Positron–electron Hylleraas-type
1	2	r_{23}	Electron–electron Hylleraas-type
2	1	$\frac{2}{R}(x_1x_2 + y_1y_2)$	Positron–electron configuration interaction (CI) product of π functions
2	2	$\frac{2}{R}(x_2x_3 + y_2y_3)$	Electron–electron CI, product of π functions

For the remaining two λ coordinates, numerical integration using Boys' boundary derivative method was used [14]. An efficient code for fast and accurate evaluation of the triple Neumann expansion integrals for general two-center applications has been published in [15].

The Born–Oppenheimer wavefunction was calculated from $R = 0.1$ to $R = 1.5$ in steps of 0.1. This range is more than sufficient for evaluating the matrix element t_{fi} (17), since the final-state wavefunction $\xi(\boldsymbol{R})$ does not extend beyond $R = 1.3$. At each R our calculation uses a different set of 200 basis functions, selected according to a procedure described in [5].

The basis functions containing r_{12} (and r_{13} by exchange) correlate the important attractive interaction between the positron and the electrons. In an earlier work, we showed that even a very limited number of basis functions of this type improves the energy significantly (see tables 2 and 3 in [16]). Further improvements were made by including basis functions of the less important electron–electron Hylleraas type and by careful optimization of the nonlinear exponents $\alpha_1, \alpha_2, \alpha_3, \beta_1, \beta_2, \beta_3$ at each R value [5].

Strasburger *et al* [17, 18] were able to obtain very accurate energy eigenvalues using basis sets of explicitly correlated Gaussians

$$\psi_i = S_{23} \exp\left[-\sum_{j=1}^{3} \alpha_j^{(i)} (\mathbf{r}_j - \mathbf{R}_j^{(i)})^2 - \sum_{j,k(j>k)}^{3} \beta_{jk}^{(i)} (\mathbf{r}_j - \mathbf{r}_k)^2 \right]. \tag{25}$$

The Gaussians cannot correctly describe the cusp in the wavefunction at zero lepton–lepton separation, while this is built into the basis used by us. Nevertheless, this can be compensated for by using sufficiently large numbers of Gaussians, and very accurate results can be obtained. In table 3, our results are compared to those in [17]. At all values of R our energies are above those in [17] and are thus less accurate. The difference is small, about 0.01 at small R and decreasing to less than 0.001 for $R = 1.5$. The calculation by Strasburger *et al* used a much larger number of basis functions (768) than was found to be practical when calculating matrix elements using our method (200 basis functions).

Using the numerically obtained wavefunction $\psi_{\text{BO}}(R; \boldsymbol{r}_1, \boldsymbol{r}_2, \boldsymbol{r}_3)$, and expressing the final-state wavefunction $\psi_{\text{Ps}}(\boldsymbol{\rho}, \boldsymbol{r}_{12})$ (15), as well as the interaction V (8), in the prolate spheroidal coordinates, the leptonic T-matrix element $t_{\text{fi}}(R)$ (17) can be obtained through a combination of analytical and numerical integrations, similar to those described above. The calculated leptonic T-matrix element $t_{\text{fi}}(R)$ calculated this way is shown by the black crosses in figure 1, for four different kinetic energies $\varepsilon_{\text{f}} = E_{\text{f}} - E_{\text{Ps}} - E_{\text{He}^+\bar{\text{p}}}$ of the outgoing Ps in the final state. An alternative way of evaluating $t_{\text{fi}}(R)$ [8, 10, 19] is to rewrite it as the product of the energy

Table 3. Leptonic energies calculated in this work compared to those calculated by Strasburger *et al* [17].

R	This work	Strasburger *et al* [17]	Difference
0.1	−0.793 4173	−0.802 8809	0.009 46
0.2	−0.832 1284	−0.841 2736	0.009 15
0.3	−0.893 2532	−0.901 8076	0.008 55
0.4	−0.973 8208	−0.981 6334	0.007 81
0.5	−1.070 4140	−1.076 8457	0.006 43
0.6	−1.178 0082	−1.182 9437	0.004 94
0.7	−1.291 7104	−1.295 5900	0.003 88
0.8	−1.407 7520	−1.410 7955	0.003 04
0.9	−1.522 8727	−1.525 2812	0.002 41
1.0	−1.634 4939	−1.636 4739	0.001 98
1.1	−1.740 9488	−1.742 5519	0.001 60
1.2	−1.841 0898	−1.842 3477	0.001 26
1.3	−1.934 1837	−1.935 2726	0.001 09
1.4	−2.020 2962	−2.021 1627	0.000 87
1.5	−2.099 3586	−2.100 1525	0.000 79

difference and the overlap between the initial and final states

$$t_{\mathrm{fi}}(R) = \left[E_{\mathrm{He}\bar{\mathrm{H}}}(R) - E_{\mathrm{He}^+\bar{\mathrm{p}}}(R) - \varepsilon_{\mathrm{f}} - E_{\mathrm{Ps}}\right] \langle \psi_{\mathrm{Ps}} \phi_{\mathrm{He}^+\bar{\mathrm{p}}} | \psi_{\mathrm{BO}} \rangle. \tag{26}$$

Results calculated using this form can also be found in figure 1. When the more accurate potential $E_{\mathrm{He}\bar{\mathrm{H}}}(R)$ calculated by Strasburger *et al* [17] is used the agreement with the direct integration is very good at all energies, the largest relative error is 8%, but in most cases it is much less. When the less accurate potential obtained from our calculation is used in (26), the discrepancy is somewhat larger. This is particularly true at short R and low energies, where the inaccuracies in the potential (see table 3) are largest. However, when the inaccuracy of the potential is smaller than ε_{f}, the $t_{\mathrm{fi}}(R)$ calculated using this form is quite accurate.

4. Elastic and hadronic annihilation cross sections

The wavefunction for nuclear motion in the initial state $\chi_{\varepsilon_{\mathrm{i}},J}$ was obtained through direct integration (using Mathematica) of the most accurate potential published by Strasburger *et al* [17]. This calculation includes both the potential and its first derivative on a grid with $\Delta R = 0.1$, which was interpolated using third-order polynomials. The potential goes through a weak maximum at $R = 2.42$. We found that the best numerical stability was obtained when the potential excluding the nuclear attraction $-2/R$ was interpolated for $R < 2.42$, while for $R > 2.42$ the $-2/R$ term was included in the interpolation. For $R > 10$ the long-range form

$$E_{\mathrm{He}\bar{\mathrm{H}}}(R) = -\frac{2.821\,3439}{R^6} - \frac{41.836\,374}{R^8} - \frac{871.540\,66}{R^{10}} \tag{27}$$

was used [20]. As the last point of the interpolation, the energy, and the derivative of the energy, obtained from (27) at $R = 10$ was used. In this way, the transition between the calculated values of the potential and the long-range form becomes smooth. At $R = 10$, the difference between the

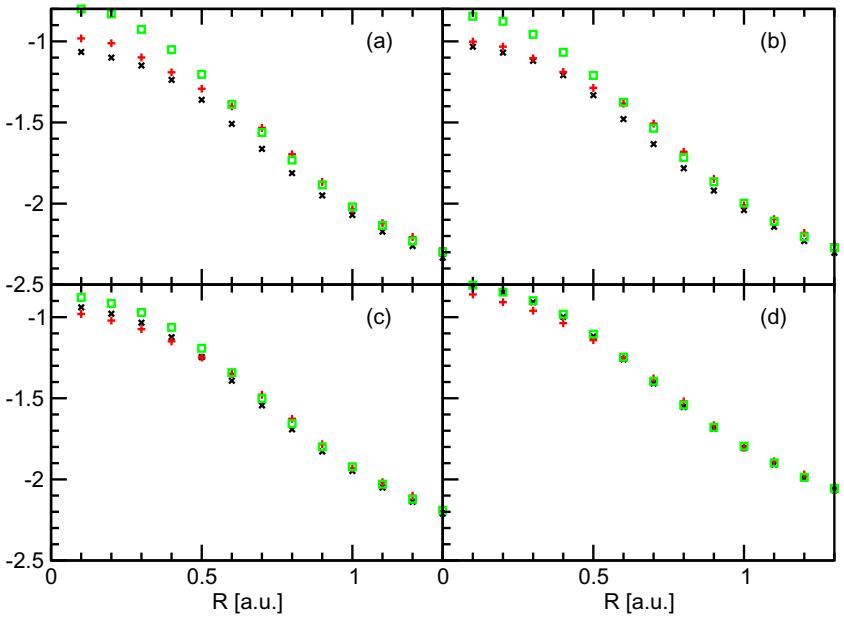

Figure 1. Leptonic T-matrix element $t_{\mathrm{fi}}(R)$ calculated using direct integration (black, $\times$), using (26) and the potential calculated in [17] (red, +), and using (26) and the potential obtained by us (green, $\square$). The different panels represent different kinetic energies in the final channel, (a) $\varepsilon_{\mathrm{f}} = 0.01$, (b) $\varepsilon_{\mathrm{f}} = 0.02$, (c) $\varepsilon_{\mathrm{f}} = 0.05$ and (d) $\varepsilon_{\mathrm{f}} = 0.10$.

value calculated in [17] and (27) is 10^{-7}. Our calculation also included the adiabatic correction to the Born–Oppenheimer potential from [17].

For initial states with non-zero angular momentum $J > 0$ the angular momentum barrier gives an effective repulsive interaction as $R \to 0$, and hence the wavefunction $\chi_{\varepsilon_{\mathrm{i}},J}$ vanishes in this limit. It is the easy to calculate $\chi_{\varepsilon_{\mathrm{i}},J}$, integrating using standard methods from $\chi_{\varepsilon_{\mathrm{i}},J}(R_0) = 0$ for some sufficiently small R_0. At large R the partial-wave phase δ_J shift can be determined from the asymptotic expansion $\chi_{\varepsilon_{\mathrm{i}},J}(R) \to \mathcal{N}\left[j_J(k_{\mathrm{i}}R) - \tan\delta_J n_J(k_{\mathrm{i}}R)\right] Y_{JM}(\hat{R})$, where j_J and n_J are the regular and irregular spherical Bessel functions and $\mathcal{N}$ is a normalization constant. The elastic cross section is then given by the standard relation

$$\sigma_{\mathrm{el}} = \sum \sigma_J, \tag{28}$$

$$\sigma_J = \frac{4\pi}{k_{\mathrm{i}}^2} \sin^2\delta_J, \quad J > 0. \tag{29}$$

For zero angular momentum, on the other hand, the potential is attractive in the limit $R \to 0$, in contrast to normal atom–atom scattering. Hence, there is a nonzero probability that the antiproton and the helium nucleus overlap, in which case they will interact through the strong nuclear force. If the effect of the strong interaction is weak the $\chi_{\varepsilon_{\mathrm{i}},0}$ can be calculated using the regular Coulomb wave $G_0(kR)$ as the short-range boundary condition. Here k has to be defined relative to the asymptote of the Coulombic interaction,

$$\frac{k^2}{2\mu} = E_{\mathrm{i}} - E^{\mathrm{PsH}}, \tag{30}$$

where E^{PsH} is the leptonic energy of the He–$\bar{\mathrm{H}}$ system in the united atom limit (equivalent to positronium hydride). In this approximation the cross section for $\bar{\mathrm{p}}$–α annihilation is proportional to the coalescence density of the two particles, i.e. $\propto |\chi_{\varepsilon_i,0}(0)|^2$ [6]. This is equivalent to first-order perturbation theory of an effective annihilation potential proportional to $\delta(\boldsymbol{R})$. As discussed in [21], this treatment is not sufficient when the strong force effects are large, as is the case for $\bar{\mathrm{H}}$–He scattering. Here a more detailed description of the strong nuclear force must be used.

We have not been able to find an effective strong-force potential for the α–$\bar{\mathrm{p}}$ interaction in the literature. Instead we use the approach based on the Coulomb-corrected strong-force scattering length, which has been described in [21]. We take advantage of the fact that the range of the strong force $R_{\mathrm{si}} \sim 10^{-5}\, a_0$ is much shorter than typical atomic distances $R_{\mathrm{a}} \sim a_0$ (here a_0 is the Bohr radius). Thus, there is a range of internuclear distances short enough for the Born–Oppenheimer potential to be completely dominated by the Coulomb attraction between the antiproton and the He nucleus, but still larger than the range of the strong nuclear interaction. In the absence of the strong interaction, the wavefunction of nuclear motion $\chi_{\varepsilon_i,J}(R)$ would in this range be proportional to the regular Coulomb function F_0. The effect of the strong interaction is, within this R-range, to add also a term proportional to the irregular Coulomb function G_0, i.e.

$$\chi_{\varepsilon_i,0}(kR) = N[F_0(kR) + \tan\delta_{\mathrm{si}} G_0(kR)], \qquad R_{\mathrm{si}} \ll R \ll R_{\mathrm{a}}. \tag{31}$$

Here δ_{si} is the phase shift induced by the strong interaction and N a normalization constant.

The strong interaction phase shift δ_{si} is a complex quantity, with its imaginary part allowing for annihilation. Taking advantage of the fact that the relevant energy scales in atomic scattering ($\sim$eV) are much smaller than typical nuclear energies ($\sim$MeV), it is enough to use the zero-energy limit of δ_{si}. In this limit δ_{si} is related to the Coulomb-corrected scattering length of the strong interaction through

$$\frac{1}{a_{\mathrm{si}}} = -\frac{2\pi}{b_\mu} \lim_{k\to 0} \cot\delta_{\mathrm{si}}(k), \tag{32}$$

where $b_\mu = -1/(2\mu)$ is the Coulomb parameter [22]. In our calculations, we have used the value $a_{\mathrm{si}} = (1.851 - 0.630\mathrm{i})$, fm $= (3.5 - 1.2\mathrm{i}) \times 10^{-5}$, which was determined by the fit to experimental low-energy $\bar{\mathrm{p}}$–He scattering data in [23].

Using the form (31) as a short-range boundary condition the interaction potential can be integrated using usual methods. As $R \to \infty$ a *complex* phase shift is obtained for the atom–antiatom scattering process. The imaginary part of the phase shift signifies annihilation, and hence depletion of the entrance channel. With a complex s-wave scattering phase shift $\delta^{J=0} = \delta_r^{J=0} + \mathrm{i}\delta_i^{J=0}$ the corresponding scattering matrix element is $S^{J=0} = \exp(2\mathrm{i}\delta^{J=0}) = \eta_0 \exp(2\mathrm{i}\delta_r^{J=0})$, where $\eta_0 = \exp(-2\delta_i^{J=0})$ is the inelasticity which expresses the loss of flux, or absorption, between the initial and final channels [9]. The s-wave part of the elastic cross section then becomes

$$\sigma_{\mathrm{el}}^{J=0} = \frac{\pi}{k_{\mathrm{i}}^2} \left|S^{J=0} - 1\right|^2 = \frac{4\pi\eta_0}{k_{\mathrm{i}}^2} \left(\sin^2\delta_r^{J=0} + \sinh^2\delta_i^{J=0}\right), \tag{33}$$

and the annihilation cross section is

$$\sigma_{\mathrm{a}} = \frac{\pi}{k_{\mathrm{i}}^2} \left(1 - \left|S^{J=0}\right|^2\right) = \frac{\pi}{k_{\mathrm{i}}^2} \left(1 - \eta_0^2\right). \tag{34}$$

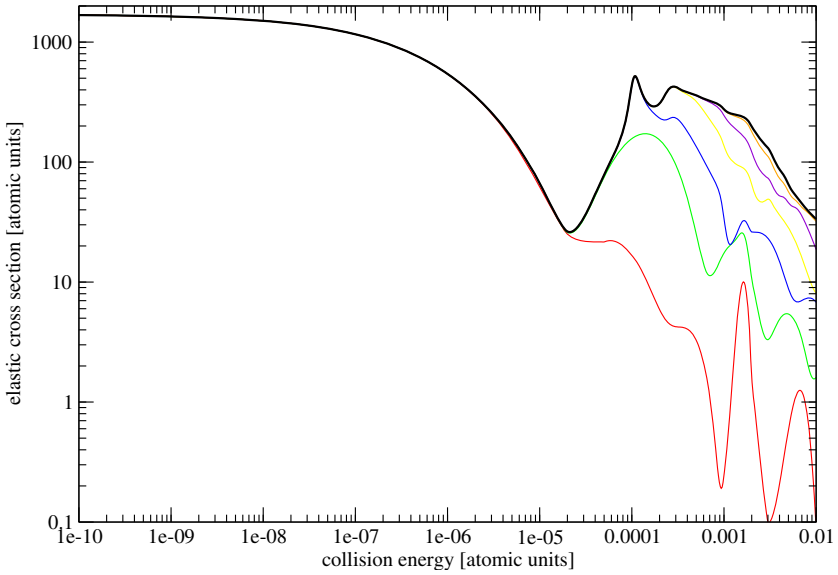

Figure 2. Convergence of the elastic cross section with the number of partial waves included in the calculation. The curves include (from below) only $J = 0$ (red), $J \leqslant 2$ (green), $J \leqslant 4$ (blue), $J \leqslant 6$ (yellow), $J \leqslant 8$ (violet), $J \leqslant 10$ (orange) and $J \leqslant 11$ (black).

5. Results

The initial-state Born–Oppenheimer wavefunction was obtained using the HeH̄ potential calculated by Strasburger *et al* [17] for collision energies between 10^{-10} and 10^{-2} (in temperature units this corresponds to between $32\,\mu$K and 3200 K, thus covering well the experimentally relevant range). At lower energies the cross sections are determined by threshold laws (see below). The calculations included partial waves up to $J = 11$. The results for the elastic cross section are displayed in figure 2.

The elastic cross section is dominated by s-wave scattering up to a collision energy $\sim 10^{-5}$ (3.2 K). In the limit of zero collision energy the $J = 0$ phase shift $\delta^{J=0} \to -ka$, where a is the scattering length, as required by threshold laws. We obtain for the scattering length $a = 2.15 - 11.4\mathrm{i}$, which gives for the elastic cross section in the zero-energy limit $\sigma_{\mathrm{el}} = 4\pi|a|^2 = 1700$. We note that the imaginary part of the scattering length is larger in magnitude than the real part. This shows that the strong interaction also has a large impact on the elastic scattering properties in the zero-energy limit. At larger collision energies, on the other hand, where higher partial waves dominate, the effects of the strong interaction are negligible. This demonstrates the extreme sensitivity of the cross section in the ultracold domain. For this reason, a very accurate potential is required to obtain reliable cross sections in this limit. An earlier calculation [24], using a slightly less accurate potential [18], obtained a different result from the present calculation. Comparing the two calculations we have determined that the main reason for the inaccurate result in [24] was that the potential in [18] was defined on an insufficiently dense grid in the region $R = 0$–2.

The elastic cross section has a resonant peak around the collision energy $\varepsilon_{\mathrm{i}} = 10^{-4}$. This is due to a shape resonance trapped behind the $J = 4$ rotational barrier (see figure 3). The

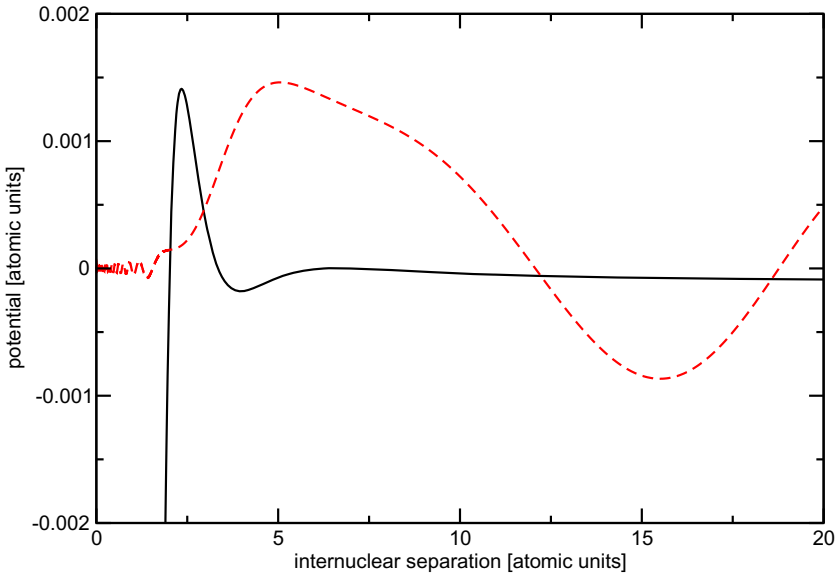

Figure 3. The wavefunction at the energy $E_r = 1.04 \times 10^{-4}$ of the shape resonance in the $J = 4$ partial wave (red, - - - -) together with the potential including the $J = 4$ rotational barrier (black, ——). (Due to the rotational barrier, the potential is again repulsive at internuclear separations less than 0.0034, which is not visible in the graph.)

interaction potential has a double-well structure when the rotational barrier is included. An inner deep well at $R < 2$ is strongly dominated by the $\bar{p}$–α attraction. At larger internuclear separations there is a shallow outer well around $R \sim 4$. The height of the barrier separating the two wells is only 3×10^{-6} for the $J = 0$ partial wave, but is reinforced when the rotational barrier is added, to 0.0015 for $J = 4$. Fitting the phase shift gives the resonance parameters as $E_r = 1.04 \times 10^{-4}$ and $\Gamma_r = 3.40 \times 10^{-5}$. The resonance energy lies only about 10^{-6} below the outer maximum of the potential barrier. This shallow outer well only exists for $J \leqslant 5$. For $J \leqslant 3$ it supports bound states, while for $J = 5$ it is too shallow to support any state.

The angular distribution of the elastic scattering is shown for various energies in figure 4. At low energies the cross section is isotropic, as expected from the dominance of the s-wave. At higher energies the scattering is mostly in the forward direction, meaning that less momentum is transferred between the colliding atoms. If the antihydrogen is initially stationary in the laboratory frame, while the helium atom hits it with a laboratory energy $\mathcal{E}^i_{\mathrm{He}}$, the amount of kinetic energy transferred to the antihydrogen atom is related to the COM scattering angle through

$$\mathcal{E}^{\mathrm{f}}_{\bar{\mathrm{H}}} = \frac{2m_{\bar{\mathrm{H}}}m_{\mathrm{He}}}{(m_{\bar{\mathrm{H}}} + m_{\mathrm{He}})^2}(1 - \cos\theta)\mathcal{E}^i_{\mathrm{He}}, \tag{35}$$

where θ is the scattering angle in the center-of-mass frame. It is therefore useful to define the momentum transfer cross section

$$\sigma_{\mathrm{mt}} = \int_0^{2\pi}\int_0^{\pi} \frac{\mathrm{d}\sigma}{\mathrm{d}\Omega}(\theta)(1 - \cos\theta)\sin\theta\,\mathrm{d}\theta\,\mathrm{d}\varphi. \tag{36}$$

This momentum transfer cross section is shown in figure 5. The resonant structure around 10^{-4} (32 K) gives a large increase in the momentum transfer. At low energies the momentum transfer

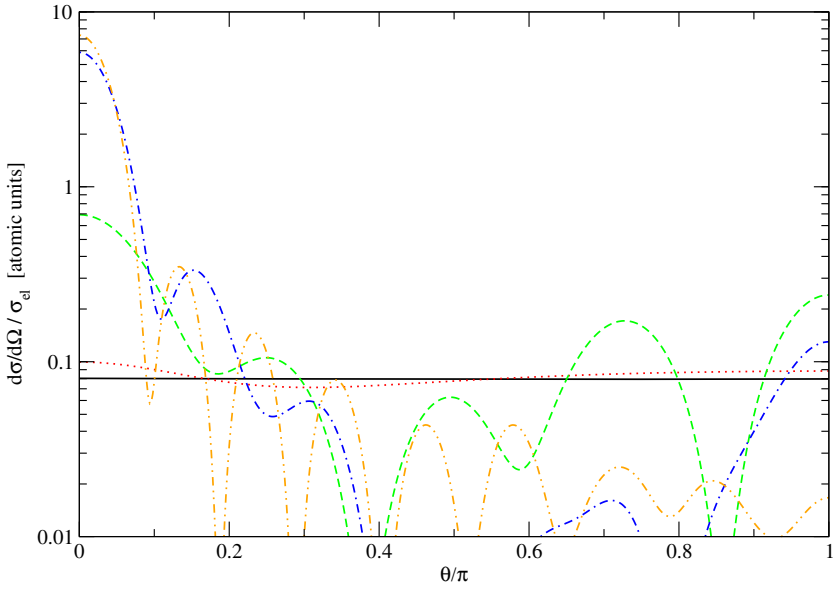

Figure 4. The angular distribution of elastic scattering $\frac{d\sigma}{d\Omega}(\theta)/\sigma_{el}$ at collision energies 10^{-6} (black, ——), 10^{-5} (red, · · · ·), 10^{-4} (green, - - - -), 10^{-3} (blue, —·—) and 10^{-2} (orange, —··—).

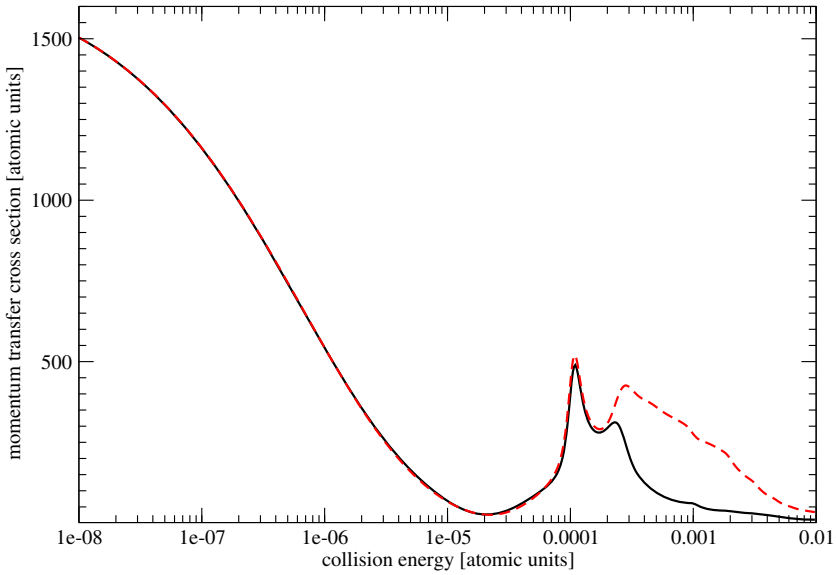

Figure 5. The momentum transfer cross section (36) as a function of collision energy (black, ——), plotted together with the total elastic cross section (red, - - - -).

cross section coincides with the total elastic cross section, while around 2×10^{-5} (6.3 K) and above 10^{-3} (320 K) the momentum transfer cross section is very small.

Turning to inelastic processes we display the cross section for rearrangement and direct annihilation in figure 6. In the same figure, we have included the total elastic and the total inelastic cross sections. We find that the direct annihilation is the dominating inelastic channel

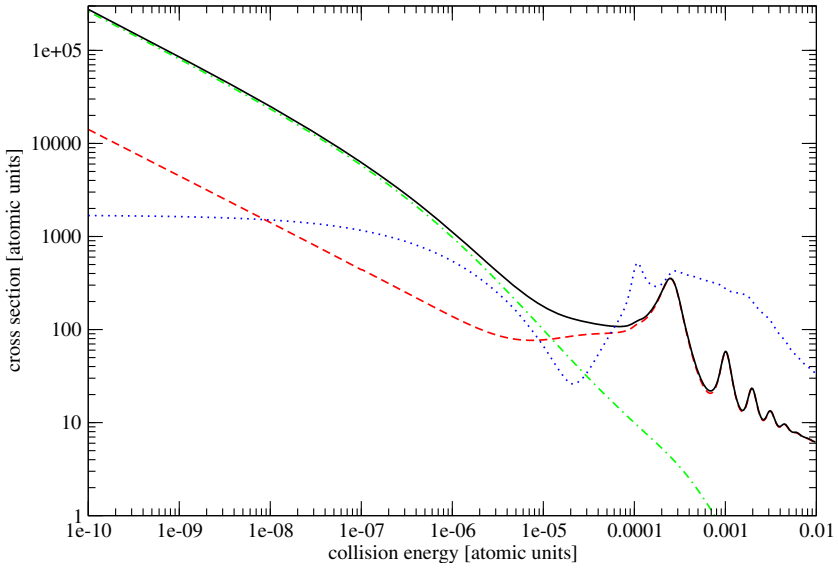

Figure 6. Cross sections for helium–antihydrogen scattering, total inelastic (black, ——), rearrangement (red, - - - -), direct annihilation (green, —·—) and total elastic (blue, · · · ·).

at energies below 1.24×10^{-5} (3.9 K). In the limit of zero collision energy the annihilation cross section approaches $2.62/\sqrt{\varepsilon_\mathrm{i}}$, while the rearrangement cross section approaches $0.14/\sqrt{\varepsilon_\mathrm{i}}$.

Another inelastic process is electron–positron annihilation. We make a simple estimate of this process based on the non-relativistic annihilation rate $4\pi c r_0^2 n_e$, where $r_0 = 2.82 \times 10^{-15}$ m is the classical radius of the electron, c is the speed of light and n_e is the coalescence density between the electrons and the positron [25]. In atomic units this expression becomes $4\pi\alpha^3 n_\mathrm{e}$, where α is the fine-structure constant. In the context of atom–antiatom scattering we have to average n_e over internuclear configurations, and divide by the flux in the initial channel, in order to convert the rate to a cross section. Using the normalization $\exp(\mathrm{i}\boldsymbol{k}_\mathrm{i} \cdot \boldsymbol{R})$ for the incoming wave, the expression for the cross section becomes

$$\sigma_a^{e^+e^-} = 4\pi\alpha^3 \sqrt{\frac{\mu}{2\varepsilon_\mathrm{i}}} \sum_J \int P(R) \left|\chi_{\varepsilon_\mathrm{i},J}(R)\right|^2 \mathrm{d}\boldsymbol{R}, \tag{37}$$

where $P(R) = 2\int |\psi_\mathrm{BO}(R; \boldsymbol{r}_1, \boldsymbol{r}_2, \boldsymbol{r}_3)|^2\, \delta(\boldsymbol{r}_1 - \boldsymbol{r}_2)\, \mathrm{d}\boldsymbol{r}_1\, \mathrm{d}\boldsymbol{r}_2\, \mathrm{d}\boldsymbol{r}_3$ is the average electron–positron overlap. $P(R)$ has been calculated by Strasburger [12], and was found to be less than twice the value for Ps, $(8\pi)^{-1}$, at all R, and falling to zero for R greater than a few atomic units. We have not calculated the integral in (37) but estimate the cross section to be of the order $\sigma_a^{e^+e^-} \sim 4\pi\alpha^3\sqrt{\mu/(2\varepsilon_\mathrm{i})} \sim 10^{-4}/\sqrt{\varepsilon_\mathrm{i}}$. This is consistent with the results $\sigma_a^{e^+e^-} = 4 \times 10^{-5}/\sqrt{\varepsilon_\mathrm{i}}$ obtained for H–$\bar{\mathrm{H}}$ scattering [26]. Our estimate for electron–positron annihilation is four orders of magnitude smaller than the cross section for nuclear annihilation. Hence, this process can be neglected.

The rearrangement cross section includes, for each J, only rearrangement to the most loosely bound $\mathrm{He}^+\bar{\mathrm{p}}$ level. While, in general, rearrangement to deeply bound states should have much smaller cross sections, it has been found for the case of H–$\bar{\mathrm{H}}$ scattering that the second most loosely bound state has the largest cross section [27]. To check whether this may also

be true in He–$\bar{\text{H}}$ scattering we have calculated the rearrangement to the second and third most loosely bound states in the zero-energy limit (see table 1). Whereas the assumption that the center-of-mass motion of the outgoing Ps is dominated by the s-wave part may be questionable for these states, the order of magnitude should still be correct. We find the cross sections $2.6\times10^{-4}/\sqrt{\varepsilon_\mathrm{i}}$ for $v = 34$ and $9.2\times10^{-3}/\sqrt{\varepsilon_\mathrm{i}}$ for $v = 33$. Since these cross sections are much smaller than for the $v = 35$ final state, we have not found a full calculation of these final states warranted.

Inelastic scattering dominates over elastic scattering at energies below 6.1×10^{-5} (19 K). The resonance at 1.04×10^{-4} is not clearly visible in the rearrangement cross section. The reason is clear from figure 3. Rearrangement only takes place from internuclear separations $R < 1.3$. In this region, the resonant enhancement of the wavefunction is moderate, since it is separated from the quasi-bound state in the shallow outer well by a barrier. Above the resonance the inelastic and elastic cross sections are again comparable around 2.5×10^{-4} (80 K), before the inelastic cross section drops off.

6. Conclusions

We have found that the double barriers in the Born–Oppenheimer potential for the He–$\bar{\text{H}}$ system with $J > 0$ give a complicated structure to the elastic and inelastic cross sections. In particular, a broad resonance at the collision energy 1.04×10^{-4} strongly influences the elastic cross section. The sum of the inelastic cross sections as well as the momentum transfer cross section goes through a minimum around 2×10^{-5}–8×10^{-5}. This corresponds to a temperature around 6–25 K. Thus, if the lifetime of trapped antihydrogen is due to collisions with He atoms, a lot can be gained by ensuring that the temperature of the background gas does not lie above ∼25 K.

In the limit of zero collision energy, we find that the strong nuclear force has a large impact on the collision process. The cross section for direct annihilation is $2.62/\sqrt{\varepsilon_\mathrm{i}}$, which can be compared to about $0.14/\sqrt{\varepsilon_\mathrm{i}}$ for H–$\bar{\text{H}}$ scattering [8, 28]. Also the zero-energy limit of the elastic cross section $\sigma_\mathrm{el} = 1700$ is almost twice as large as for H–$\bar{\text{H}}$. The rearrangement cross section, on the other hand, approaches $0.14/\sqrt{\varepsilon_\mathrm{i}}$, which is less than the corresponding cross sections $0.67/\sqrt{\varepsilon_\mathrm{i}}$ [27] and $1.1/\sqrt{\varepsilon_\mathrm{i}}$ [19] reported for H–$\bar{\text{H}}$. Hence, at zero energy, annihilation dominates over rearrangement for the He–$\bar{\text{H}}$ system, while the opposite is true for H–$\bar{\text{H}}$.

The elastic scattering cross section is less than the sum of the inelastic processes for energies below 19 K, and again is also comparable at higher energies. Thus, schemes for cooling antihydrogen using laser-cooled atoms do not seem suitable for helium, since at the relevant temperatures antihydrogen atoms will be lost rather than cooled.

Acknowledgment

This research was supported by the UK EPSRC and the Swedish Research Council (VR).

References

[1] Andresen G B *et al* 2010 *Nature* **468** 673
[2] Enomoto Y *et al* 2010 *Phys. Rev. Lett.* **105** 243401
[3] ALPHA collaboration 2011 *Nature Phys.* **7** 558
[4] Andresen G B *et al* 2010 *Phys. Rev. Lett.* **105** 013003

[5] Armour E A G, Todd A C, Jonsell S, Liu Y, Gregory M R and Plummer M 2008 *Nucl. Instrum. Methods Phys. Res.* B **266** 363
[6] Jonsell S, Saenz A, Froelich P, Zygelman B and Dalgarno A 2001 *Phys. Rev.* A **64** 052712
[7] Strasburger K 2004 *J. Phys. B: At. Mol. Opt. Phys.* **37** 4483
[8] Jonsell S, Saenz A, Froelich P, Zygelman B and Dalgarno A 2004 *J. Phys. B: At. Mol. Opt. Phys.* **37** 1195
[9] Joachain C 1975 *Collision Theory* (Amsterdam: North-Holland)
[10] Armour E A G and Jonsell S 2007 *J. Phys. A: Math. Gen.* **40** 701
[11] Frolov A M and Smith V H Jr 1997 *Phys. Rev.* A **55** 2662
[12] Strasburger K 2004 *J. Phys. B: At. Mol. Opt. Phys.* **37** 2211
[13] Usukura J, Varga K and Suzuki Y 1998 *Phys. Rev.* A **58** 1918
[14] Armour E A G and Humberston J W 1991 *Phys. Rep.* **204** 165
[15] Plummer M, Armour E A G, Todd A C, Franklin C P and Cooper J N 2009 *Comput. Phys. Commun.* **180** 2410
[16] Armour E A G, Jonsell S, Liu Y and Todd A C 2006 *Nucl. Instrum. Methods Phys. Res.* B **247** 127
[17] Strasburger K, Chojnacki H and Sokolowska A 2005 *J. Phys. B: At. Mol. Opt. Phys.* **38** 3091
[18] Strasburger K and Chojnacki H 2002 *Phys. Rev. Lett.* **88** 163201
[19] Zygelman B, Saenz A, Froelich P and Jonsell S 2004 *Phys. Rev.* A **69** 042715
[20] Bishop D M and Pipin J 1993 *Int. J. Quantum Chem.* **45** 349
[21] Jonsell S, Saenz A, Froelich P, Zygelman B and Dalgarno A 2005 *Can. J. Phys.* **83** 435
[22] Trueman T L 1961 *Nucl. Phys.* **26** 57
[23] Gal A 2002 *Nucl. Phys.* A **699** 300
[24] Jonsell S, Froelich P, Eriksson S and Strasburger K 2004 *Phys. Rev.* A **70** 062708
[25] Ferrell R A 1956 *Rev. Mod. Phys.* **28** 308
[26] Froelich P, Jonsell S, Saenz A, Eriksson S, Zygelman B and Dalgarno A 2004 *Phys. Rev.* A **70** 022509
[27] Armour E A G and Chamberlain C W 2002 *J. Phys. B: At. Mol. Opt. Phys.* **35** L489
[28] Armour E A G, Liu Y and Vigier A 2005 *J. Phys. B: At. Mol. Opt. Phys.* **38** L47